Synthesis of Superelastic Compliant Mechanisms for Target Shape Matching

Hargrove, Brianne A.; Frecker, Mary; Jovanova, Jovana

DOI
10.1109/ReMAR61031.2024.10617613

Publication date
2024

Document Version
Final published version

Published in
Proceedings of the 6th International Conference on Reconfigurable Mechanisms and Robots, ReMAR 2024

2024 6th International Conference on Reconfigurable Mechanisms and Robots (ReMAR)
June 24-27, 2024. Chicago, IL, USA

Synthesis of Superelastic Compliant Mechanisms for Target Shape Matching

Brianne A. Hargrove[1], Mary Frecker[2], and Jovana Jovanova[3]

2024 6th International Conference on Reconfigurable Mechanisms and Robots (ReMAR) | 979-8-3503-9596-9/24/$31.00 ©2024 IEEE | DOI: 10.1109/REMAR61031.2024.10617613

Abstract— **The design freedom of the additive manufacturing (AM) process has created new avenues for compliant mechanisms to have more complex geometries, functionality, and mechanical behavior than conventional manufacturing methods offer. However, the challenge in the assumption of "free complexity" in AM is the trial-and-error often involved in creating a design that behaves as intended. To address this problem, a synthesis method incorporating nonlinear-elastic materials and large deformations as geometric nonlinearity is proposed, using an assembly of building blocks to construct a compliant mechanism. Designs generated by the model illustrate the optimization of the building block selection, size, shape, and topology to achieve different deflected states. The combination of the superelastic behavior of shape memory alloys such as Nitinol, and the exploration of different building block geometries, has been shown to enhance the flexibility of the optimized mechanism to reach such target shapes.**

I. Introduction

Compliant mechanisms (CMs) rely on the elastic deformation of their flexible components to transfer force, motion, and energy. The response of a mechanism is largely driven by the individual members of the CM, such as size and shape, the arrangement or final topology, the choice of material, and constraints on the stress, weight, and volume of the design [1]. Analysis of the force-deflection response of CMs, for example, requires a prescribed set of geometric and mechanical parameters. Yet, for inverse design or synthesis, these parameters may be difficult for the designer to select without trial-and-error and prototyping.

To address this issue, CM synthesis has become automated over the years through structural optimization to compute the optimal size, shape, and topology that meet a specific objective(s). Numerical algorithms have been developed for continuum-based CM synthesis using techniques such as homogenization-based optimization [2], as well as for multicriteria optimization using a layout of interconnected truss elements or ground structure [3]. Earlier optimization models were often limited to small deformations. Researchers incorporated the method of moving asymptotes [4,5], and later, genetic algorithms in path-generation CM synthesis [6,7] and nonlinear springs approximated by compliant splines [8], along with the ability to capture large deformations. Other methods for synthesis have been presented based on kinematics such as rigid body replacement to represent compliance with flexure joints [9], or in the case of the pseudo rigid body model (PRBM) [10,11] and finite-spring-link model [12], with torsional springs.

A more recent approach entails the use of basic elements known as building blocks. Parallel connections of elastic beams represented by compliance ellipsoids have been employed in synthesis of planar CMs undergoing small deflections [13,14]. Flexure-based CM synthesis for both serial and parallel connections of compliant building elements have also been explored using screw theory and the matrix method [15]. In the area of metal AM, building blocks defined by linear and circular curve profiles have been studied to synthesize spatial, self-supported CMs [16].

These methods present a framework for topology synthesis, or the arrangement and orientation of building blocks, but the optimization of the size and shape at the elemental level has not been considered. An optimization-based algorithm, the Nelder-Mead method, was implemented into the shape and topology optimization of large stroke flexure mechanisms to identify the removal and replacement of building blocks that produce unwanted natural frequencies [17]. Still, a limitation of the previous building block methods is that they are restricted to linear-elastic material behavior, which severely limits the selection pool of materials for additively manufactured CMs.

Combined with large deformations, the introduction of material nonlinearity in the design of CMs allows for a controlled and tailorable response, especially when considering hyperelastic and superelastic materials that are available with various mechanical properties and can recover large amounts of elastic deformation [18]. The development of a synthesis method that includes these two sources of nonlinearity could allow for greater material exploration beyond typically used stiff plastics and metals. Thus, the goal of this work is to synthesize large-deflection, nonlinear-elastic CMs using building blocks. The optimization scheme presented in [17] is similar, but we consider planar mechanisms. To explore nonlinear-elasticity, this paper is

*Research supported by Leighton Riess Professorship in Engineering at Penn State University.

[1]Brianne. A. Hargrove is with the Department of Mechanical Engineering, Penn State, University Park, PA 16802, USA (e-mail: bbh5128@psu.edu).

[2]Mary Frecker is with the Department of Mechanical Engineering, Penn State, University Park, PA 16802, USA (e-mail: mxf36@psu.edu).

[3]Jovana Jovanova is with the Departments of Mechanical, Maritime, and Materials Engineering, Transport Engineering and Logistics, TU Delft, Delft, Mekelweg 5, 2628 CD, Netherlands (e-mail: J.Jovanova@tudelft.nl).

focused on studying a shape memory alloy (SMA) material model of superelastic Nitinol (NiTi) that exhibits tension-compression asymmetry in the stress-strain response. The *patternsearch* solver in MATLAB is selected as the optimization algorithm in that it is faster than stochastic methods like the genetic algorithm (GA). But, the GA is considered as a global search strategy as *patternsearch* may converge to a local optimum. Using this algorithm, the CMs are optimized to match a target shape for a given loading condition. The target shape is defined using a segmentation approach, which converts the profile into a predefined number of control points within the design space. Target shape optimization has been considered for the synthesis of shape-changing rigid body mechanisms defined by morphing curves [19], for CMs made from functionally-graded SMAs [20], for lithium-ion battery actuators [21], and magnetoactive elastomer actuators [22].

The following sections present the proposed optimization methodology for CM synthesis for target shape matching, the building block library considered in the assembly of the CM, and case studies highlighting the exploration of size, shape, and topology optimization to match different target shapes. The analytical model developed in [23] is used to assess the force-deflection behavior of the optimized CM in achieving the defined target shape.

II. Design Optimization Algorithm

A. Objective Function and Design Variables

To match a desired shape, the shape error between the deflected CM shape and the target shape is minimized. In other words, the target shape is segmented using control points (c_p) that fall on the surface as shown in Fig. 1.

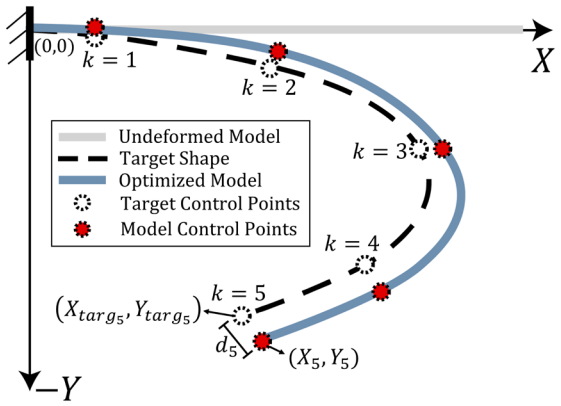

Figure 1. Example of a target shape segmented using 5 control points and the Eucledian distance (d_k) between nearby points on the optimized design.

The shape error (e) is defined as the sum of the minimum Eucledian distance between these control points and nearby points on the deflected CM. The distance equation is given by Eq. (1) and the corresponding shape error by Eq. (2).

$$d_k = \sqrt{\left(X_k - X_{targ_k}\right)^2 + \left(Y_k - Y_{targ_k}\right)^2} \quad \text{for } k = 1, \dots, c_p \tag{1}$$

$$e = \sum_1^{c_p} d_k \tag{2}$$

Three penalty functions are incorporated into the objective function to enforce constraints. The first two are constraints placed on the maximum stress in the CM, and the third constraint is on the maximum length of the design. The first stress constraint limits the maximum tensile and compressive stresses in the CM to lie within the upper and lower bounds of the stress-strain curve for a given material. In the consideration of NiTi as the material, the addition of a second stress constraint also ensures that the maximum tensile and compressive stress is within the superelastic range, such that when the load is removed, the mechanism recovers its original shape. The superelastic range is between the first and second critical stresses $\sigma_1^{(t,c)^*}$ and $\sigma_2^{(t,c)^*}$. The length constraint confines the horizontal or vertical dimension of the CM, depending on the orientation, to a maximum value. Depending on the desired design, the length constraint (L_{des}) can be changed to scale the size of the mechanism. The penalty functions are defined using a quadratic loss function, as given in Eq. (3), where either a penalty of zero is added or the squared difference.

$$\begin{aligned} \sigma_{p_1} &= \max\left[0, \left(\sigma_{max} - \sigma_2^{t^*}\right)^2\right] + \\ &\max\left[0, \left(|\sigma_{min}| - |\sigma_2^{c^*}|\right)^2\right], \\ \sigma_{p_2} &= \max\left[0, \left(\sigma_1^{t^*} - \sigma_{max}\right)^2\right] + \\ &\max\left[0, \left(|\sigma_1^{c^*}| - |\sigma_{min}|\right)^2\right] \text{ and} \\ L_p &= \max[0, (L_{des} - L_{max})\text{^}2] \end{aligned} \tag{3}$$

The objective function is then expressed as a weighted error function, with weights w_1, w_2, and w_3 in Eq. (4).

$$e' = e + w_1\sigma_{p_1} + w_2\sigma_{p_2} + w_2 L_p \tag{4}$$

The objective function e' used in the design problem for target shape matching is now considered. The sum of the weights should equal to 1, i.e., $w_1 + w_2 + w_3 = 1$. As such, the weights can be equal to 1/3 or varied such that their sum still equals to 1. The weighting factors are selected by the designer based on their relative importance. For the analytical model, the minimization of the objective function is dependent on the individual segments that make up the CM geometry in terms of their size, shape, connectivity. These segments are referred to as building blocks, which are constructed from basic beam elements. The types of elements studied in this approach are based on initially straight and initially curved beams, as also explored in [13], and will be presented collectively as a building block library.

One of the most critical design variables involves the selection of a building block from the building block library that best meets the objective. The library has a total of 8 building blocks that are available for selection by the optimization model. Each building block (BB) is assigned an integer value that serves as an identifier in the assembly. As a result, the choice of building block is a design variable. The maximum number of building blocks that can be used in the assembly is given by an integer value of n. The in-plane half thickness (b_i), length (L_i), and in the case of certain building blocks, the angle of rotation (γ_i) and the sector angle (α_i) are

also design variables. The index, i, corresponds to a segment within a given building block and has a value of either 1 or 2. Given these parameters, the optimization problem is formally introduced by Eq. (5).

$$\begin{aligned} \text{Minimize} \quad & e' \\ \textit{subject to} \quad & 1 \le BB \le 8 \\ & 1 \le \#BBs \le n \\ & b_{min} \le b_i \le b_{max} \\ & L_{min} \le L_i \le L_{max} \\ & \gamma_{min} \le \gamma_i \le \gamma_{max} \\ & \alpha_{min} \le \alpha_i \le \alpha_{max} \end{aligned} \tag{5}$$

To understand the function of the design variables in the definition of a building block, and later their assembly, the building block library is presented next.

III. Building Block Synthesis

A. Building Block Library Characterization

A building block library was defined for the synthesis using a collection of beam elements. The development of the library aimed to include beam geometries beyond the initially straight beam such that complex target shapes could be studied. As such, the library is categorized by four building blocks considering solely initially straight beams, as shown in Fig. 2, as well as four building blocks constructed from beams with initial curvature. The first group of building blocks builds upon a single initially straight beam (BB_1) as the basic element. Two beams are then assembled to form "dyads" where the individual lengths (L_1, L_2), in-plane half thicknesses (b_1, b_2), and angle of rotation or orientation with respect to the horizontal axis (γ_1, γ_2) are included as design variables. The second building block (BB_2) represents when the angle of rotation of the beam elements is equal, but of opposite sign. The third (BB_3) adds variation in the second angle of rotation, by removing the equality condition. The fourth building block (BB_4) represents an angled beam connected to a horizontal beam, where only the first angle of rotation is optimized. The out-of-plane thickness is assumed to remain constant for all building blocks and their derivatives.

The second group of the library consists of beams with initial curvature. In this case, the angle of rotation (γ_i) is prescribed, and instead the sector angle (α_i) of the beam is a design variable. The addition of the sector angle affects only BB_5 and BB_6 that are based on initially curved beams, where α_1 and α_2 are optimized. In the case of the third building block, which is referred to as the "3" beam based on its shape, the sector angle is set to 180° to represent a semicircular arc. Likewise, the sector angle for the "S" beam is also predefined to obtain two semicircular arcs with inverse initial curvatures. For all building blocks, the lengths and in-plane half-thicknesses are optimized by the model. To reduce the number of design variables, the building blocks share the same optimized values of $L_1, L_2, b_1, b_2, \gamma_1, \gamma_2, \alpha_1$, and α_2.

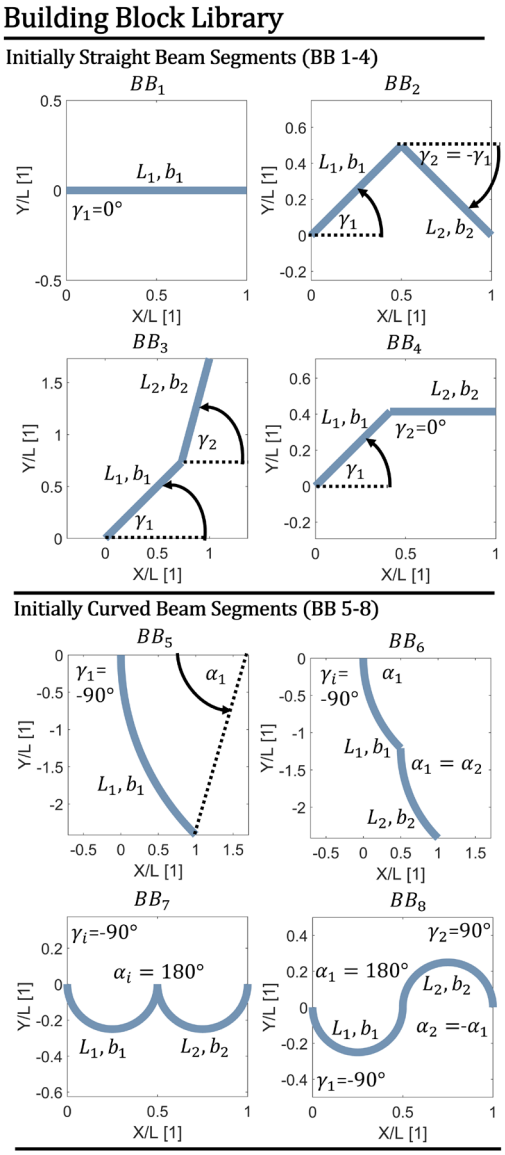

Figure 2. Building block library categorized by intially straight and initially curved beams, with 8 building blocks available in total.

With the building block library defined, along with the respective design variables of each building block, the criteria for the selection of a specific building block to be used in the CM design will be discussed for a single-objective optimization algorithm.

B. Optimization Scheme

The optimization algorithm uses *patternsearch* (PS) in MATLAB to determine the optimal CM design. First, the algorithm is initialized with a randomized feasible design. The objective function is evaluated for this initial design, and if it does not satisfy the fitness limit, it locates a new potential design. In terms of the building block selection, the design is initialized with n segments. For $n = 5$, the solver could produce a solution with two dyads and a single beam element, a solution with 5 beam elements, or a single dyad connected to 3 beam elements. The discrete variable BB is optimized between 1 and 8, such that for a given position in the CM, BB is tuned iteratively toward a building block that improves the

fitness at that location. The solver does not create solutions that violate the maximum number of possible building blocks defined by n. The deformation of the building blocks is analyzed using the segmented beam model derived in [23], where the local deformation of the individual building blocks is rotated and transformed to the global coordinate system.

C. Superelastic Material Model

The material model chosen for the building block synthesis is a model for superelastic NiTi with tension-compression asymmetry, as presented in detail in [23], and does not consider the unloading of the material or the temperature-induced shape memory effect. For this work, only stresses up to the superelastic region of NiTi are used so that the shape can be recovered after the removal of the load. Fig. 3 shows the material model for superelastic NiTi, which is approximated using a multilinear model with 2 linear sections. A future iteration of the proposed approach will explore the addition of the mechanical properties like the elastic moduli $\left(E_1^{(t,c)}, E_2^{(t,c)}\right)$ and critical stresses $\left(\sigma_1^{(t,c)^*}, \sigma_2^{(t,c)^*}\right)$ as design variables. Other material models can also be studied to further generalize the approach. The following section presents three case studies of the application of the synthesis method incorporating both the nonlinear-elastic NiTi model and large deformations for different target shapes.

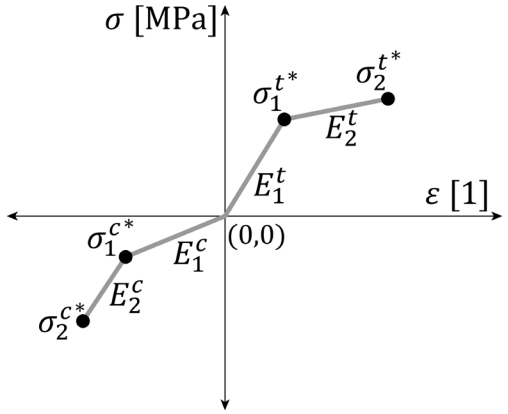

Figure 3. Superelastic multilinear material model for asymmetric NiTi.

IV. Results

In this section, the building block synthesis method is illustrated for three CM designs. The first is a deployable accordion array that could be applied to foldable, origami compliant mechanisms. In this case, the design is restricted to only initially straight building blocks (*BB* 1-4). The second case study is for the design of a compliant mechanism comprised of solely initially curved building blocks (*BB* 4-8), that illustrates the superelasticity and large shape-change behavior of the mechanism. The last case study looks at a fixed-guided beam that considers the full building block library (*BB* 1-8) and highlights the effect of the number of building blocks on the accuracy of the optimized design. For the three case studies, the current state of the model prescribes the mechanical properties of NiTi with the values shown in Table I.

TABLE I. ASYMMETRIC NITI MECHANICAL PROPERTIES

Property	Values	
	Tensile (t)	*Compressive (c)*
E_1 [GPa]	69.2	50
E_2 [GPa]	15.0	29.1
σ_1^* [MPa]	900	-500
σ_2^* [MPa]	1500	-1200

The lower and upper limits on the design variables for the algorithm are given by Table II. The weights (w_1, w_2, w_3) are set to the same value of 1/3 in Eq. (4).

TABLE II. BOUNDS FOR DESIGN VARIABLES

Design Variables	Values	
	Lower Bound	*Upper Bound*
BB	1	8
$\#BBs$	1	10
b_i [mm]	5	10
L_i [mm]	50	200
γ_i [deg]	-90	90
α_i [deg]	-180	180

For the PS algorithm, the fitness limit is 1E-3. '*GSSPositiveBasis2N*' is used as the poll method and a nonuniform *patternsearch* (NUPS) algorithm is employed to search the mesh space. A mesh tolerance of 1E-6 is also used as a measure to terminate the algorithm if the desired fitness is not reached. It is also possible for PS to converge to a local optimum due to the initial guess of the design variables, or starting points, and deterministic nature of the solver. This can be remedied by restarting the solver using different or randomized starting points, or also by adding the genetic algorithm as a secondary search strategy to drive the solver toward the global optimum. The advantages of hybridized approaches using the GA as a global search strategy, and refinement through PS for local exploration to reduce the computational time of the GA are reported in [24–26]. As a result, the '*searchga'* option is included.

A global search using the GA is done at the first iteration of the PS until a suitable fitness value is reached, in this case, 1E-2. Then, PS continues to refine the search locally at the termination of '*searchga'* towards a more optimal solution. The parameters for the genetic algorithm include a population size of 200, a maximum number of generations of 100, a mutation rate of 0.01, and a crossover ratio of 0.7. The optimization model in MATLAB was run on a computer with an Intel Core i7-11800H processor running at 2.30GHz, with 8 available cores for parallel computing, 16 logical processors, a GeForce RTX 3070 graphics card, and 32 GB RAM.

A. Deployable Accordion

The target shape is represented by two control points along the same line, as shown in Fig. 4. The maximum desired length of the design (L_{des}) is selected as 300 mm. As such, the *X* and *Y* coordinates in the global coordinate system are presented as a dimensionless value with respect to the desired length, i.e., X/L_{des} and Y/L_{des}. The length of the accordion model is defined in a vertical orientation, leading to the building block library being rotated by 90°. To evaluate the extent to which the deflected optimized design satisfies the target shape, the model is subject to a downward force of 5 kN at its tip on the topmost horizontal segment. The bottom

and top building blocks are prescribed with a length of 100 mm, an in-plane half thickness of 5 mm, and an out-of-plane thickness of 50 mm.

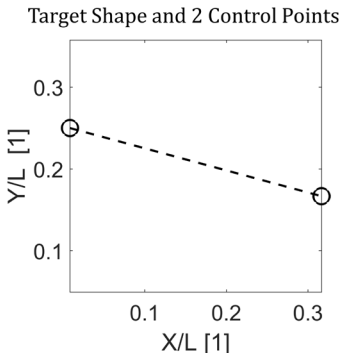

Figure 4. Target shape for deployable accordion with 2 target points.

To minimize the shape error, the algorithm begins with a randomized guess that evolves to the optimized design as shown in Fig. 5(a). For this example, the design variables include the number of building blocks, the building block itself from the library, the in-plane thickness, and the angle of rotation in the case of a dyad. The length is not included as a design variable initially, and it is shown that the shape error is poor, i.e., the optimized geometry does not hit all of the target points when deformed. In Fig. 5(b), the length is now included as a design variable. It can be seen that when using only the PS algorithm to optimize the design, it converges to a local optimum. As a result, the '*searchga'* function is added to PS to improve the solution, where both target points are met with a series of dyad building blocks.

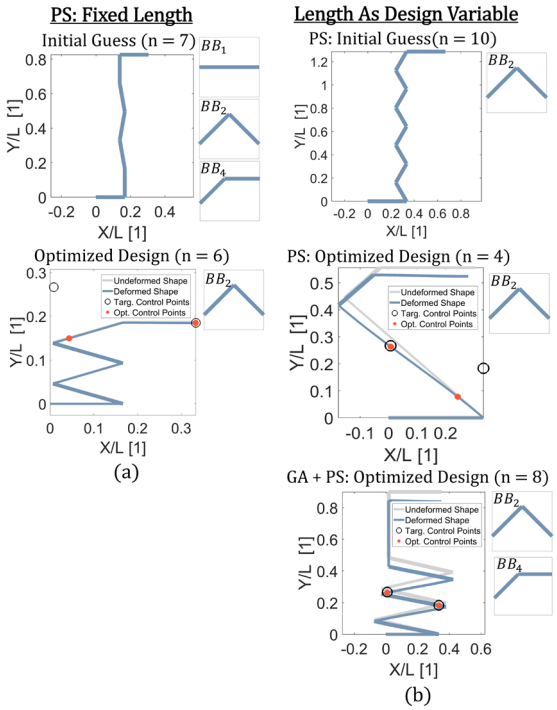

Figure 5. Optimized acordion designs using only PS algorithm given a fixed length of 50 mm (a) and with the length as a design variable (b), where the addition of the 'searchga' function improves the convergence of patternsearch to a more optimal solution.

Tables III and IV show the optimized design variables for the deployable accordion when the length of the building blocks is fixed and when the length is a design variable, respectively. The shape error is also presented to highlight the improvement of the objective function with the addition of '*searchga'* in Table IV. The deformation of the accordion was kept small in this case to first validate that the algorithm could select the appropriate building blocks for the design problem. However, the next example accounts for superelasticity in a larger range of deformation. Due to the improvement in the shape error by the '*searchga'* function, it is used in the remaining examples as well.

TABLE III. OPTIMIZED DESIGN VARIABLES FOR ACCORDION DESIGN WITH FIXED LENGTH AND SHAPE ERROR

Design	Design Variables					Error
	n	BBs	b_1 [mm]	b_2 [mm]	γ_1 [°]	e'
Initial Guess	7	[1,2,4]	5.0	5.0	80.0	9.1E-2
Final (PS)	6	2	5.2	5.0	16.3	3.6E-2

TABLE IV. OPTIMIZED DESIGN VARIABLES FOR ACCORDION DESIGN WITH LENGTH AS DESIGN VARIABLE AND *BBS = 2 FOR ALL DESIGNS*

Design	Design Variables						Error
	n	b_1 [mm]	b_2 [mm]	L_1 [mm]	L_2 [mm]	γ_1 [°]	e'
Initial Guess	10	5.0	5.0	55	55	60	9.7E-2
Final (PS)	4	5.0	6.1	197	50	42.4	4.10E-2
Final (GA+PS)	8	5.2	5.2	124	138	12.9	1.82E-4

B. *Curved Compliant Mechanism*

The creation of a curved CM based on initially curved building blocks is performed for two different target shapes. The first target shape is an 'S' geometry and the second is a '3' geometry, as shown in Fig. 6. Both shapes are defined by 5 control points. The '3' target shape builds upon the complexity on the S shape by testing whether the model can match shape imposed with different lengths. The length of the model is defined in a horizontal orientation, and the maximum desired length is chosen to be 100 mm. The out-of-plane thickness is 50 mm. The tip of the CM is subject to a counterclockwise moment of 1 kNm.

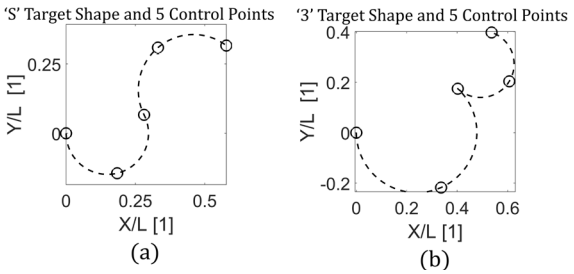

Figure 6. Target shapes for curved mechanism with 5 target points for 'S' (a) and '3' (b) geometries.

The results in Figure 7 show the optimized curved mechanism design first for the 'S' target shape. In the two cases, the algorithm selects $n = 3$ building blocks to be the

optimal number for the assembly. First, the model is optimized for a smaller number of target points ($c_p = 3$). The target shape is obtained using a combination of the 'S' building block, which is expected based on the target, and an initially curved beam in Fig. 7(a). Then, the model was reevaluated using more target points ($c_p = 5$) in Fig. 7(b). The design achieves a much larger range of deformation such that the maximum stresses at the fixed end lie within the superelastic region of the NiTi material model. Similarly, superelasticity is exploited to obtain the '3' target shape of Fig. 7(c), which utilize the '3' building block and an initially curved beam (BB_5). The 'S' design that matches the 3 target points has the smallest shape error, as defined in Table V, potentially resulting from less control points that need to be matched and a simpler target shape.

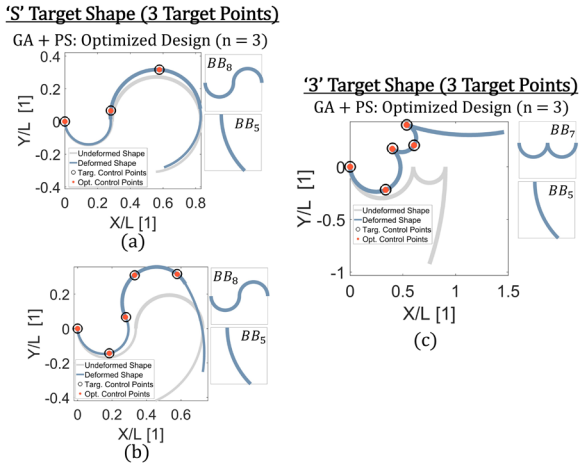

Figure 7. Optimized curved mechanism designs using PS algorithm + searchga for an 'S' target shape with 3 control points (a) and 5 control points (b), and a '3' target shape with 5 control points (c).

TABLE V. OPTIMIZED DESIGN VARIABLES FOR CURVED MECHANISM DESIGN USING SEARCHGA AND PATTERNSEARCH ALGORITHM WITH 3 BUILDING BLOCKS

Design	Design Variables						Error
	BBs	b_1 *[mm]*	b_2 *[mm]*	L_1 *[mm]*	L_2 *[mm]*	α_1 *[°]*	e'
'S' (3 points)	[8,5]	6.3	10.0	45.3	85.5	83.9	6.9E-4
'S' (5 points)	[8,5]	4.4	7.3	53.1	60.9	66.4	8.5E-4
'3' (5 points)	[7,5]	4.4	4.4	93.9	48.0	18.7	1.7E-3

Of note in performing these case studies is understanding why the inclusion of nonlinear-elasticity (NLE) and large deformations (LD) in the synthesis is important. When simplifying assumptions of small deformations and/or material linearity are made, the design may not meet the target shape when considering the actual nonlinear behavior. In the following example, the force-deflection response of the proposed model is assessed using a design optimized with the assumption of linear-elasticity (LE) and small deformations (SM), and also with linear-elasticity and large deformations.

When linear-elasticity and small deformations are assumed, the method generates a design that meets some of the control points of the '3' target shape. However, when that design is evaluated considering nonlinear-elasticity and large deformations in the analytical model, the shape error is poor, i.e., the deformed shape no longer agrees well with the target shape as seen in Fig. 8(a) and (b). Likewise, when linear-elasticity and large deformations are assumed, the deformed shape matches some of the target points in Fig. 8(c). However, when evaluated for the actual nonlinear mechanical response, the shape error worsens in Fig. 8(d). As a result, the development of this nonlinear-elastic synthesis method for large deformations is necessary for synthesizing designs that accurately capture the behavior of the material and geometry selected.

As a final demonstration of the optimization model, the last case study looks at the creation of a fixed-guided mechanism and the effect of the number of building blocks on the accuracy of the optimized design.

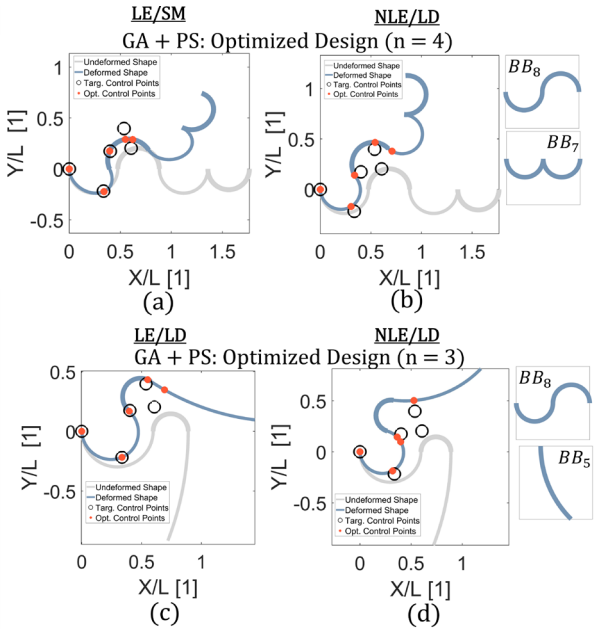

Figure 8. Optimized curved mechanisms illustrating differences in shape error for assumptions of LE/SM (a) and LE/LD (c) against NLE/LD (b, d).

C. *Fixed-Guided Mechanism*

The fixed-guided mechanism is intended to show an application of compressive loading that, in the future, will be applied as a quarter-symmetric model of a unit cell that is compressed axially at its center. In this example, the algorithm selects from the full library of building blocks. The desired target shape is shown in Fig. 9 with 4 control points. The model is oriented horizontally, and the maximum desired length is chosen to be 300 mm. The out-of-plane thickness is 50 mm. The tip of the CM is loaded with a downward force of 20 kN and a reaction moment that is a function of the applied force and the horizontal tip coordinate, $M_R = F_y l/2$. The reaction moment constrains the slope at the tip of the CM to be horizontal, but there is no constraint on the axial deformation of the CM.

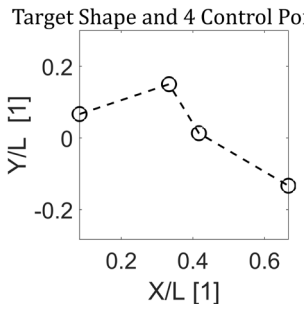

Figure 9. Target shape for a fixed-guided mechanism.

To study the effect that the number of building blocks (n) has on the value of the shape error, n is removed as a design variable in the following example. Instead, n is an input within the range of 1 to 4 building blocks total. As presented in Fig. 10(a), the design with only 1 building block has the largest shape error. However, with increasing building blocks, the deformed shape gets closer to the target points as shown in Fig. 10(b), (c), and (d). With the exception of Fig. 10(d), where the initially curved beam has a sector angle of α_1= -9.3°, the algorithm selects initially straight building blocks as the optimal in the assembly.

It is noted that the solver arrives at designs that match the target points, but not necessarily the target shape as in the case of the curved mechanism. In other words, the algorithm finds a different design that still meets the prescribed target points. Overall, the synthesis method generates designs that agree well with the given target points, accounting for a nonlinear-elastic material model and large deformations. It has been shown that the method is successful at iteratively refining the arrangement of building blocks, as well as their size and shape, to minimize the objective without designer input.

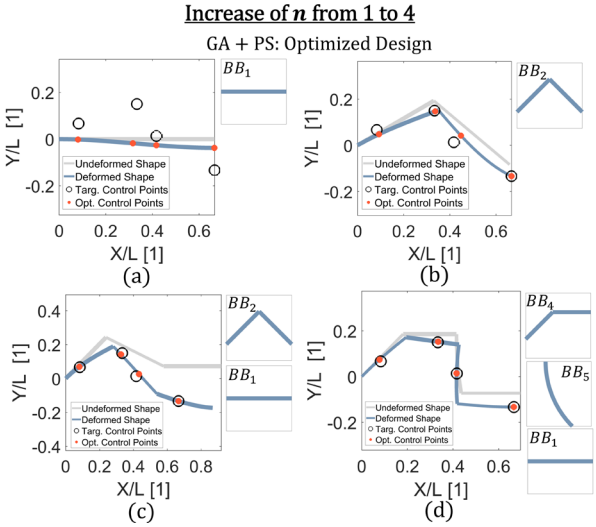

Figure 10. Optimized fixed-guided mechanism with the number of building blocks set as n = 1 (a), n = 2 (b) n = 3 (c), and n = 4 (d).

TABLE VI. OPTIMIZED DESIGN VARIABLES FOR FIXED-GUIDED MECHANISM DESIGN USING SEARCHGA AND PATTERNSEARCH ALGORITHM WITH PRESCRIBED NUMBER OF BUILDING BLOCKS

Design	Design Variables						Error
	BBs	b_1 *[mm]*	b_2 *[mm]*	L_1 *[mm]*	L_2 *[mm]*	γ_1 *[°]*	e'
n = 1	1	8.6	-	200	-	-	1.1E-1
n = 2	2	7.0	5.9	109	138	-33	2.3E-2
n = 3	[2,1]	7.1	6.9	102	114	-46	2.3E-2
n = 4	[4,5, 1]	7.9	9.0	78	70	-46	1.9E-2

V. CONCLUSION

This work has presented an optimization methodology of CM synthesis for large deformations using nonlinear-elastic building blocks. Given a variety of target shapes and points, the model assembles CMs that minimize the shape error. In terms of manufacturing of the CMs, the synthesis method has the potential for selecting additive manufacturing parameters that are informed by an optimization model instead of by trial-and-error, prototyping, and iteration. A future version of the model will explore the addition of material selection as a design variable. Also, methods will be introduced to remove and replace building blocks that worsen the fitness function to further improve the convergence of the algorithm to optimal solutions.

ACKNOWLEDGMENT

The authors would like to acknowledge the Penn State Leighton Riess Chair in Engineering.

REFERENCES

[1] Hetrick, J. A., and Kota, S., 1999, "An Energy Formulation for Parametric Size and Shape Optimization of Compliant Mechanisms," ASME. J. Mech. Des., **121**(2).

[2] Bendsøe, M. P., and Kikuchi, N., 1988, "Generating Optimal Topologies in Structural Design Using a Homogenization Method," Comput Methods Appl Mech Eng, **71**(2), pp. 197–224.

[3] Frecker, M. I., Ananthasuresh, G. K., Nishiwaki, S., Kikuchi, N., and Kota, S., 1997, "Topological Synthesis of Compliant Mechanisms Using Multi-Criteria Optimization," ASME. J. Mech. Des., **119**(2), pp. 238–245.

[4] Bruns, T. E., and Tortorelli, D. A., 2001, "Topology Optimization of Non-Linear Elastic Structures and Compliant Mechanisms," Comput Methods Appl Mech Eng, **190**(26–27), pp. 3443–3459.

[5] Pedersen, C. B. W., Buhl, T., and Sigmund, O., 2001, "Topology Synthesis of Large-Displacement Compliant Mechanisms," Int J Numer Methods Eng, **50**(12), pp. 2683–2705.

[6] Saxena, A., 2005, "Synthesis of Compliant Mechanisms for Path Generation Using Genetic Algorithm," Journal of Mechanical Design, **127**(4), pp. 745–752.

[7] Mankame, N. D., and Ananthasuresh, G. K., 2007, "Synthesis of Contact-Aided Compliant Mechanisms

for Non-Smooth Path Generation," Int J Numer Methods Eng, **69**(12), pp. 2564–2605.
[8] Jutte, C. V., and Kota, S., 2008, "Design of Nonlinear Springs for Prescribed Load-Displacement Functions," J. Mech. Des., **130**(8), p. 081403.
[9] Su, H. J., Shi, H., and Yu, J., 2012, "A Symbolic Formulation for Analytical Compliance Analysis and Synthesis of Flexure Mechanisms," J. Mech. Des., **134**(5), p. 051009.
[10] Murphy, M. D., Midha, A., and Howell, L. L., 1996, "The Topological Synthesis of Compliant Mechanisms," Mech Mach Theory, **31**(2), pp. 185–199.
[11] Mattson, C. A., Howell, L. L., and Magleby, S. P., 2004, "Development of Commercially Viable Compliant Mechanisms Using the Pseudo-Rigid-Body Model: Case Studies of Parallel Mechanisms," J Intell Mater Syst Struct, **15**(3), pp. 195–217.
[12] Saggere, L., and Kota, S., 1997, "Synthesis of Distributed Compliant Mechanisms for Adaptive Structures Application: An Elasto-Kinematic Approach," Proceedings of the ASME 1997 Design Engineering Technical Conferences, Volume 2: 23rd Design Automation Conference, Sacramento, California, USA., **2**, p. V002T29A027.
[13] Kim, C. J., Moon, Y.-M., and Kota, S., 2008, "A Building Block Approach to the Conceptual Synthesis of Compliant Mechanisms Utilizing Compliance and Stiffness Ellipsoids," J. Mech. Des., **130**(2), p. 022308.
[14] Zhang, J., Guo, H. W., Wu, J., Kou, Z. M., and Eriksson, A., 2022, "Design of Flexure Revolute Joint Based on Compliance and Stiffness Ellipsoids," Proc Inst Mech Eng G J Aerosp Eng, **236**(4), pp. 623–635.
[15] Li, C., and Chen, S.-C., 2023, "Design of Compliant Mechanisms Based on Compliant Building Elements. Part I: Principles," Precis Eng, **81**, pp. 207–220.
[16] Danun, A. N., Palma, P. D., Klahn, C., and Meboldt, M., 2021, "Building Block Synthesis of Self-Supported Three-Dimensional Compliant Elements for Metallic Additive Manufacturing," Journal of Mechanical Design, **143**(5), p. 053301.
[17] Fix, M. E., Brouwer, D. M., and Aarts, R. G. K. M., 2020, "Building Block Based Topology Synthesis Algorithm to Optimize the Natural Frequency in Large Stroke Flexure Mechanisms," Proceedings of the ASME 2020 International Design Engineering Technical Conferences and Computers and Information in Engineering Conference, Virtual, Online, **2**, p. V002T02A007.
[18] Hargrove, B., Nastevska, A., Frecker, M., and Jovanova, J., 2022, "Pseudo Rigid Body Model for a Nonlinear Folding Compliant Mechanism," Mech Mach Theory, **176**, p. 105017.
[19] Zhao, K., Schmiedeler, J. P., and Murray, A. P., 2012, "Kinematic Synthesis of Planar, Shape-Changing Rigid-Body Mechanisms With Prismatic Joints," Proceedings of the ASME Design Engineering Technical Conference, Washington, DC, USA, **6**, pp. 523–533.
[20] Jovanova, J., Frecker, M., Hamilton, R. F., and Palmer, T. A., 2019, "Target Shape Optimization of Functionally Graded Shape Memory Alloy Compliant Mechanisms," J Intell Mater Syst Struct, **30**(9), pp. 1385–1396.
[21] Gonzalez, C., Shan, S., Frecker, M., and Rahn, C., 2021, "1D Shape Matching of a Lithium-Ion Battery Actuator," Proceedings of the ASME 2021 Conference on Smart Materials, Adaptive Structures and Intelligent Systems, Virtual, Online, p. V001T01A002.
[22] Pan, T., Leng, R., Uitz, O., Seepersad, C., Ounaies, Z., and Frecker, M., 2023, "Analytical Modeling of a Magnetoactive Elastomer Unimorph," Smart Mater Struct, **32**(9), p. 095021.
[23] Hargrove, B., Frecker, M., Nastevska, A., and Jovanova, J., 2024, "An Analytical Model for Nonlinear-Elastic Compliant Mechanisms with Tension-Compression Asymmetry," J Mech Robot, **16**(12), p. 121006.
[24] Lok, C. L., Vengadaesvaran, B., and Ramesh, S., 2017, "Implementation of Hybrid Pattern Search–Genetic Algorithm into Optimizing Axial-Flux Permanent Magnet Coreless Generator (AFPMG)," Electrical Engineering, **99**, pp. 751–761.
[25] Keskin, K., and Engin, O., 2021, "A Hybrid Genetic Local and Global Search Algorithm for Solving No-Wait Flow Shop Problem with Bi Criteria," SN Appl Sci, **3**, p. 628.
[26] Payne, J. L., and Eppstein, M. J., 2005, "A Hybrid Genetic Algorithm with Pattern Search for Finding Heavy Atoms in Protein Crystals," Proceedings of the 7th annual conference on Genetic and evolutionary computation, GECCO 2005, Washington DC, USA, pp. 377–384.